Spectral link and macroscopic non-universality in turbulent plane Couette flow

Dongrong Zhang

School of Mathematics and Physics, University of South China, Hengyang, China 421001

Okinawa Institute of Science and Technology Graduate University, Onna, Okinawa, Japan 904-0495

E-mail: zdrzeo@gmail.com

April 2019

Abstract. In fully developed turbulent plane Couette flow the classical experimental data of frictional factor f vs. Reynolds number Re display well-known disparities which have long remained unexplained. These disparities are accompanied by previously unnoticed disparities in the wakes, and only in the wakes, of the attendant mean-velocity profiles (MVPs). To help explain these experimental data, we apply the model of the "spectral link" for MVPs to turbulent plane Couette flows. The model links the dissipative range, the inertial range, and the energetic range of the standard phenomenological model of the spectrum of turbulent kinetic energy to, respectively, the buffer layer, the log layer, and the wake of the MVPs. By assessing the empirical data using the spectral model, we argue for the existence, in plane Couette flow, of multiple states of turbulence which differ from one another only at the largest lengthscales in the flow, corresponding to the energetic range, where the spectrum is subject to finite-domain effects. Thus, the multiplicity of turbulent states is entirely consistent with small-scale universality, and the experimental data on plane Couette flow pose no challenge to the phenomenological theory of turbulence. Our findings might apply more broadly to a general class of flows engendered by moving boundaries.

Keywords: turbulent plane Couette flow, friction factor, mean-velocity profile, spectral link, macroscopic non-universality, small-scale universality

1. Introduction

The classical experiments on turbulent plane Couette flow date back to the 1950s, to the independent experiments by Reichardt (1956, 1959) and by Robertson (1959). These classical experiments focused on the friction factor f. A dimensionless measure of the wall shear stress τ_0, the friction factor is defined as $f \equiv \tau_0/\rho u_c^2$, where $u_c \equiv u(y = b)$, that is, the mean velocity u evaluated at the centerline of the flow, $y = b$, where b is half the thickness of the gap between the plates ‡.

From the onset, the experiments revealed a conspicuous disparity in the relation between f and the Reynolds number $\mathrm{Re} \equiv u_c b/\nu$ (Fig. 1), where ν is the kinematic viscosity of the fluid. In consultation with Reichardt, Robertson repeated his experiments but the disparity prevailed and has never been resolved (Robertson and Johnson; 1970). Later, more experiments became available, including the experiments by Telbany and Reynolds (1982), whose measurements of f are in good accord with Reichardt's, and the experiments by Kitoh et al. (2005), whose measurments of f agree well with Robertson's. In the meantime, direct numerical simulations (DNS) of turbulent plane Couette flow became possible. Remarkably, the computational f–Re relation turns out to be quite distinct from either of the experimental f–Re relations (Fig. 1). At the same value of Reynolds number Re, the friction factors of Robertson (1959) and Kitoh et al. (2005) are consistently higher than those of Reichardt (1959) and Telbany and Reynolds (1982), but consistently lower than the computational ones.

The Reichardt–Robertson disparity has always been thought of as an anomaly, the inadvertent product of a systematic error that would sooner or later be identified and factored in. The implicit notion has been that to each value of Re there should correspond a unique turbulent state and, therefore, a unique value of f.

In view of Fig. 1, we argue that this notion should be abandoned. Thus, in what follows, we shall accept as a fact the experimental and computational evidence that to each value of Re there might actually correspond multiple values of f. Furthermore, we shall assume that each one of these values of f signals a specific, alternative turbulent state.

A number of questions are then brought to the fore: How are we to characterize a turbulent state? In what ways do various turbulent states differ among themselves? Can the existence of multiple turbulent states be reconciled with the phenomenological theory of turbulence?

Before we seek to answer these questions, we turn our attention to the mean-velocity profiles (MVPs) of turbulent plane Couette flow. The MVPs have been ignored in discussions of the Reichardt–Robertson disparity. And yet, the friction factor f is closely related to the MVPs (Furuichi et al.; 2015), and the disparities in the f–Re

‡ In plane Couette flow the fluid is confined between two mutually parallel plates which move parallel to one another at a constant relative velocity. Here, we will consider the frame of reference in which the lower plate is stationary. No pressure gradient is imposed on the fluid; thus the total shear stress is uniform across the thickness and coincides with τ_0.

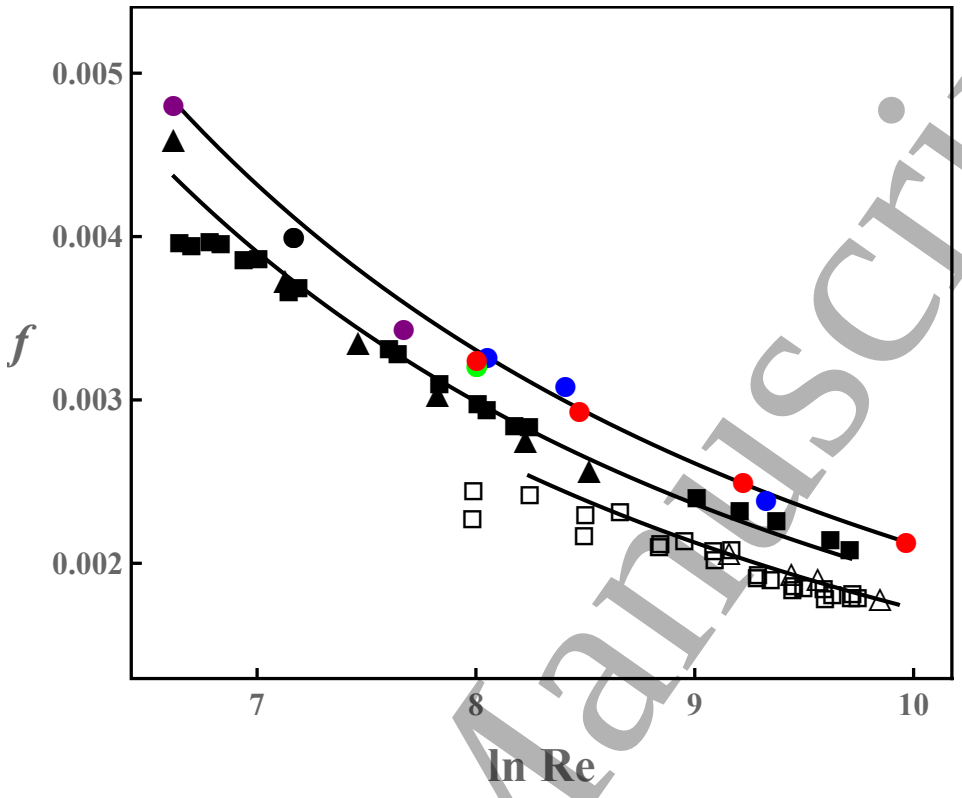

FIG. 1. Log-linear plots of experimental and computational data on the relation between the friction factor f and the Reynolds number Re of turbulent plane Couette flow. □ from Reichardt (1959). △ from Telbany and Reynolds (1982). ■ from Robertson (1959). ▲ from Kitoh et al. (2005). ○ DNS from Lee and Kim (1991) (Green), Bech et al. (1995) (black), Tsukahara et al. (2006) (Purple), Avsarkisov et al. (2014) (Blue), and Pirozzoli et al. (2014) (Red), respectively. Solid lines are the empirical formulas from Telbany and Reynolds (1982): $0.0331/(\log \mathrm{Re})^2$, Robertson (1959): $0.0361/(\log \mathrm{Re})^2$, and Pirozzoli et al. (2014): $0.0399/(\log \mathrm{Re})^2$, respectively.

relation should be reflected in concomitant disparities in the MVPs, which in turn might help shed light upon the nature of the different turbulent states that prevail in turbulent plane Couette flow.

In Fig. 2, we plot the MVPs for the highest Re available in various experiments and computations, all for plane Couette flow. The MVPs are plotted in terms of the classical dimensionless "wall variables" $\tilde{y}$ and $\tilde{u}$, where $\tilde{y} \equiv u_\tau y/\nu$ and $\tilde{u} \equiv u/u_\tau$. From Fig. 2 we can verify that at similar values of Re_τ (the friction Reynolds number, an alternative form of the Re defined as $\mathrm{Re}_\tau \equiv u_\tau b/\nu$) the various MVPs are indistinguishable everywhere in the domain of the flow *except for the wake*. Indeed, the disparities in the f–Re relation are reflected in the wakes of the MVPs, *and only there*, in the form of varying degrees of overshooting of the log law.

Even though some of the values of Re_τ that appear in Fig. 2 are not entirely comparable with the others (especially for the experiment of Kitoh et al. (2005) and the computations of Avsarkisov et al. (2014), where the highest available values of Re_τ are

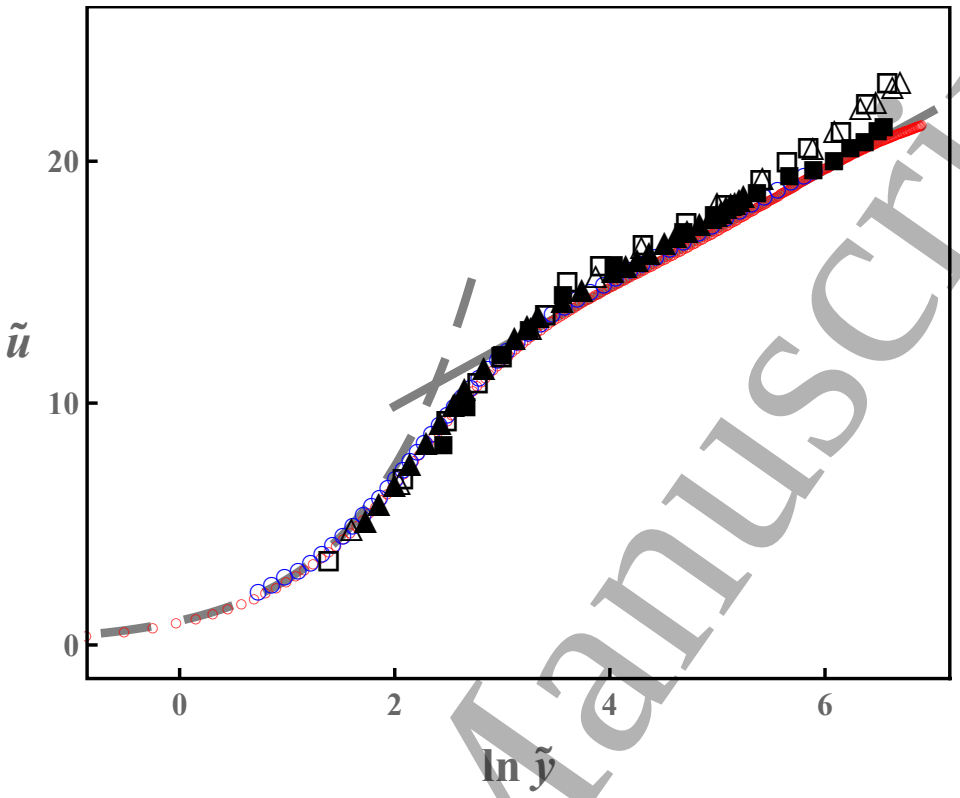

FIG. 2. Log-linear plots of experimental and computational data on the MVPs of turbulent plane Couette flow. □ $\mathrm{Re}_\tau = 723$ (Reichardt; 1959). △ $\mathrm{Re}_\tau = 805$ (Telbany and Reynolds; 1982). ■ $\mathrm{Re}_\tau = 700$ (Robertson; 1959). ▲ $\mathrm{Re}_\tau = 192$ (Kitoh et al.; 2005). ◯ DNS from (Avsarkisov et al.; 2014) (Blue) at $\mathrm{Re}_\tau = 550$, and Pirozzoli et al. (2014) (Red) at $\mathrm{Re}_\tau = 986$, respectively. The grey line denotes the "log law,"Prandtl (1953); Tennekes and Lumley (1972) $\tilde{u}(\tilde{y}) = (1/\kappa)\ln\tilde{y} + B$ with $\kappa = 0.81$ (the "Kármán constant") and $B = 5$. The dashed grey line denotes the laminar solution of the viscous layer, $\tilde{u}(\tilde{y}) = \tilde{y}$. Each MVP extends from the wall to $\tilde{y} = \mathrm{Re}_\tau$, which corresponds to the centerline of the flow. The MVPs collapse on a single curve close to the wall in the viscous layer, the buffer layer, and the log layer (where the log law prevails), while there are significant discrepancies in the wakes.

rather small), it can be clearly seen that the overshooting of the log law is largest for the experiments of Reichardt (1959) and Telbany and Reynolds (1982), second largest for the experiments of Robertson (1959), and smallest for the computations of Pirozzoli et al. (2014) (Fig. 2). That is, a higher friction factor consistently corresponds to a smaller overshooting in the wakes of the MVPs. Indeed, the overshooting can be quantified by the value of the non-dimensional velocity slope at the flow centerline, which is defined as

$$R_s \equiv \frac{b}{u_\tau}\frac{du}{dy}|_{y=b} \equiv \frac{d\tilde{u}}{d\ln\tilde{y}}|_{\tilde{y}=\mathrm{Re}_\tau}. \quad (1)$$

A higher value of R_s indicates a larger overshooting in the wakes of the MVPs. In Fig. 3 it is possible to confirm the conclusion from Fig. 2, namely that a higher friction factor consistently corresponds to a smaller overshooting in the wakes of the MVPs (if

we exclude as an outlier, likely due to scatter, the only counterexample, which occurs at a very small Reynolds number).

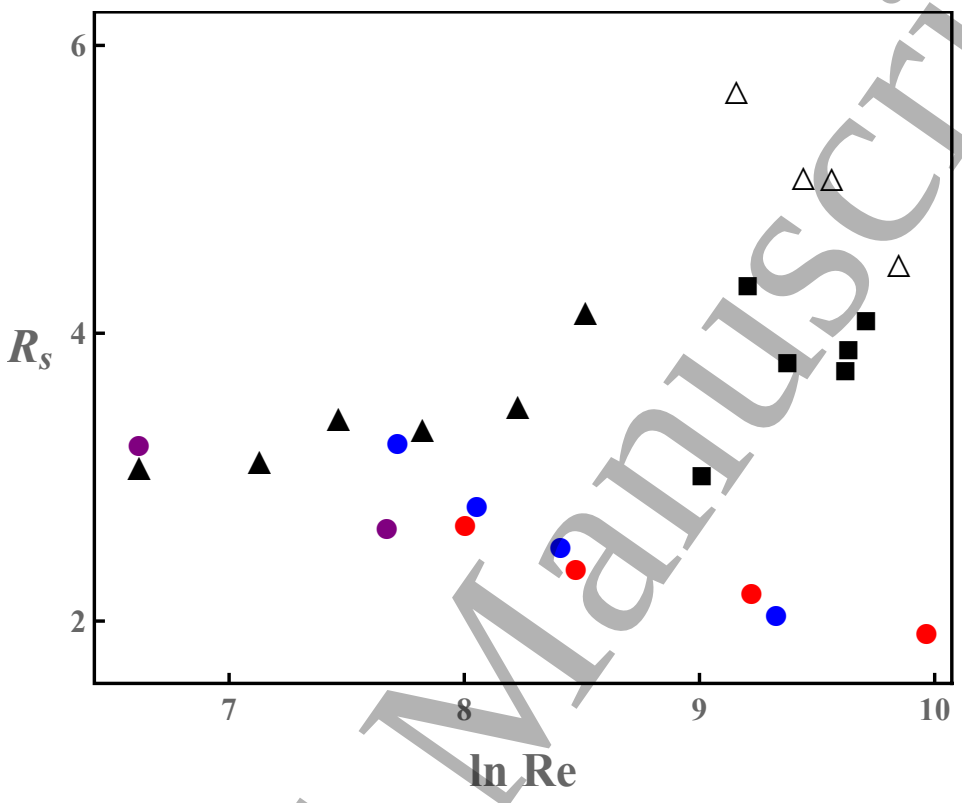

FIG. 3. Log-linear plots of experimental and computational data on the relation between the non-dimensional velocity slope at the flow centerline, R_s, and the Reynolds number Re of turbulent plane Couette flow. △ from Telbany and Reynolds (1982). ■ from Robertson (1959). ▲ from Kitoh et al. (2005). ◯ DNS from Tsukahara et al. (2006) (Purple), Avsarkisov et al. (2014) (Blue), and Pirozzoli et al. (2014) (Red), respectively.

To summarize our discussion so far: we have ascribed the disparities in the f–Re relation to the existence of multiple turbulent states in turbulent plane Couette flow. In addition, we have verified that these disparities are reflected in the wakes of the MVPs, and only there, in the form of varying degrees of overshooting of the log law. In what follows, we intend to harness this latter fact in order to explain, with help from a spectral model of the MVPs (Gioia et al.; 2010) of turbulent plane Couette flow, the way in which the multiple turbulent states differ from one another. Thus, we turn to the spectral model.

2. The model of spectral link

As a starting point of our analysis, here we outline the model of the "spectral link" for MVPs in turbulent pipe flows and channel flows (Gioia et al.; 2010). In the next section, we adapt this spectral model to turbulent plane Couette flows. The model

is grounded on the existence of a mathematical link between the MVPs and the eddy velocity distribution of the phenomenological theory of turbulence (or, alternatively, the spectrum of turbulent kinetic energy of the phenomenological theory of turbulence).

2.1. The spectrum of turbulent kinetic energy

The spectrum of turbulent kinetic energy, or the spectrum for short, is a function of the wavenumber k, $E(k)$, defined by the expression $dv_k^2/dk = E(k)$, where v_k is the characteristic velocity of a turbulent eddy of wavenumber k. Note that $k \propto 1/s$, where s is the size of the eddy; thus the eddy velocity distribution of the phenomenological theory is but a derivative of the spectrum. Indeed, the velocity of an eddy of size s, v_s, can be computed as

$$v_s = \sqrt{\int_{1/s}^{\infty} E(k)dk}, \tag{2}$$

where

$$E(k) = \frac{2}{3}(\kappa_\varepsilon \varepsilon)^{2/3} k^{-5/3} \exp(-\beta_d \eta k)(1 + (\beta_e/bk)^2)^{-17/6}. \tag{3}$$

This expression for $E(k)$ corresponds to the standard model of the spectrum. It consists of

(i) the power-law spectrum of Kolmogórov, $\frac{2}{3}(\kappa_\varepsilon \varepsilon)^{2/3} k^{-5/3}$, valid in the inertial range, where the dynamics of the turbulent eddies is dominated by the inertial forces of the energy cascade, with vanishing interference from viscous and finite-domain effects. Here, κ_ε is a dimensionless, non-negative constant which can be theoretically estimated as 4/5 (Gioia et al.; 2010; Gioia and Chakraborty; 2006), ε is the turbulent power per unit mass (that is, the characteristic invariant of the energy cascade), and $-5/3$ is the spectral exponent.

(ii) The dissipative-range correction that accounts for the effect of viscosity at high wavenumber (small eddies), $\exp(-\beta_d \eta k)$, where β_d is a dimensionless, non-negative constant known as the dissipative-range parameter, and η is the viscous lengthscale, $\eta = \nu^{3/4} \varepsilon^{-1/4}$.

(iii) The energetic-range correction that accounts for effect of finite domain at low wavenumber (large eddies), $(1 + (\beta_e/bk)^2)^{-17/6}$, where β_e is a dimensionless, non-negative constant known as the energetic-range parameter, and b is the size of the largest eddies, which size is commensurate, for plane Couette flow, with the thickness of the gap between the plates.

The standard model of the spectrum has been tested successfully by comparison with extensive measurements of the velocity fluctuations carried out over a wide range of Reynolds numbers, and by a variety of probing techniques, in laboratory flows, atmospheric flows, flows with shear and flows without shear, as well as by comparison with velocity fluctuations computed in numerical simulations (Pope; 2000). In spite of its relative simplicity, the standard model provides a comprehensive, quantitative and

physically meaningful account of each of the features of the spectrum evinced by the empirical data.

For future reference, note that $E(k) > 0$ for all k. Thus, from $v_s = \sqrt{\int_{1/s}^{\infty} E(k)dk}$, we conclude that v_s is a monotonically increasing function of s. In other words, the larger the eddy, the larger its characteristic velocity.

By substituting the standard model of the spectrum in Eq. (2), we obtain (Gioia et al.; 2010)

$$v_s = (\kappa_\varepsilon \varepsilon s)^{1/3}\sqrt{I}, \tag{4}$$

where

$$I \equiv I(\eta/s, s/b) \equiv \frac{2}{3}\int_1^{\infty} \xi^{-5/3}\mathrm{Exp}(-\xi\beta_d\eta/s)(1+(\beta_e s/b)^2/\xi^2)^{-17/6}d\xi \tag{5}$$

and $\xi \equiv sk$. In general, for an eddy of size s in the inertial range ($\eta \ll s \ll b$), $I = 1$ and $v_s = (\kappa_\varepsilon \varepsilon s)^{1/3}$, which is the eddy velocity distribution in the inertial range. For an eddy size s in the dissipative range ($s \lesssim \eta$) or the energetic range ($s \gtrsim b$), $I < 1$ and $v_s < (\kappa_\varepsilon \varepsilon s)^{1/3}$, with the implication that the eddy is *slower* than an imaginary eddy of the same size in the inertial range. Thus, the dissipative-range correction and the energetic-range correction may be said to depress the spectrum relative to the power-law spectrum of Kolmogórov. Indeed, if we set $\beta_d = \beta_e = 0$—that is, if there were no dissipative-range correction and no energetic-range correction (an unphysical proposition)—$v_s = (\kappa_\varepsilon \varepsilon s)^{1/3}$ for all s, and all eddies would be inertial.

2.2. Turbulent shear stress and spectral link

We seek to derive an expression for the turbulent shear stress that acts on a wetted surface W_y at a distance y from the wall (Fig. 4). Here we use a method different from the original derivation of Gioia et al. (2010): our derivation is grounded on the concept of control volume (CV) (Vincenti; 1982). Consider a cuboidal CV whose upper face (of surface area S) overlaps with W_y and whose lower face is at a distance y_1 from the wall. The length of the CV is X. Here, y_1 and X are arbitrary. Eddies of size s and velocity v_s bring high-momentum fluid (momentum per unit mass $\sim \rho u(y+s)$) into the CV and take low-momentum fluid (momentum per unit mass $\sim \rho u(y-s)$) out of the CV. The net momentum exchanged in a time interval Δt is

$$\Delta M \sim S v_s \Delta t\, \rho u(y+s) - S v_s \Delta t\, \rho u(y-s) \approx 2S\rho v_s \Delta t s \frac{du(y)}{dy}. \tag{6}$$

Thus, there is a turbulent force F acting on CV, $F = \Delta M/\Delta t \sim 2\rho S v_s s\, du(y)/dy$, and the turbulent shear stress τ_{t12} must be the same as this turbulent force per unit area, that is $\tau_{t12} = F/S \sim \rho s v_s\, du(y)/dy$.

Now, we have seen that v_s is a monotonically increasing function of s. Thus, τ_{t12} is also a monotonically increasing function of s, and the production of turbulent shear

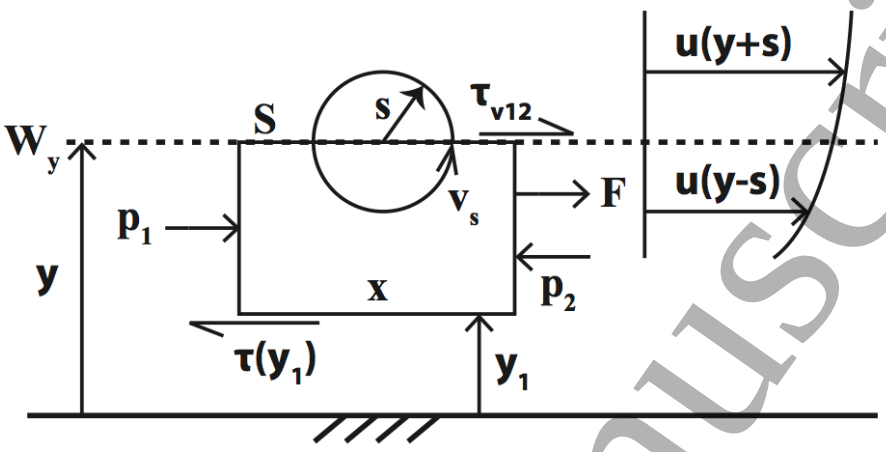

FIG. 4. Schematic used to derive an expression for the turbulent shear stress on the wetted surface W_y. For the coordinate axes, we choose the x axis to be along the streamwise direction and the y axis to be along the wall-normal direction. Note that $y = 0$ corresponds to the wall, so that W_y is at a distance y from the wall.

stress must be dominated by the largest eddies that straddle W_y—that is, the eddies of size $s = y$. We conclude that

$$\tau_{t12} = \kappa_\tau \rho y v_y \frac{du(y)}{dy}, \tag{7}$$

where κ_τ is a dimensionless proportionality constant. Next, we set $s = y$ in Eq. (4) to obtain, $v_y = (\kappa_\varepsilon \varepsilon y)^{1/3}\sqrt{I}$, where $\varepsilon = \tau_{t12}\frac{du(y)}{dy}/\rho$ is the energy equation (or, more precisely, the turbulent kinetic budget equation (Kundu and Cohen; 2002)); substituting in Eq. (7):

$$\tau_{t12} = \kappa^2 \rho I^{3/4} y^2 (\frac{du(y)}{dy})^2, \tag{8}$$

where $\kappa \equiv (\kappa_\varepsilon \kappa_\tau^3)^{1/4}$ and $I \equiv I(\eta/y, y/b)$.

Eq. (7) links the turbulent shear stress to v_y, the eddy velocity distribution, which is a function of the spectrum. In other words, Eq. (7) is the "spectral link". It was first derived (along with Eq. (8)), for turbulent pipe flow and channel flow by Gioia et al. (2010), who showed that the parameter κ in Eq. (7) is but the Kármán constant of the log law, which according to the model can be expressed as $\kappa \equiv (\kappa_\varepsilon \kappa_\tau^3)^{1/4}$. Thus, the Kármán constant is set by κ_τ and κ_ε, which relate to the mechanism of momentum transfer and to the spectrum, respectively. The fact that the Kármán constant depends explicitly on a parameter related to the spectrum, namely κ_ε, serves as a striking reminder of the fundamental *spectral* nature of the model.

3. Equations of the MVPs

For turbulent plane Couette flow, the total shear stress can be expressed in the form

$$\tau(y) = \tau_{v12} + \tau_{t12} = \tau_0. \tag{9}$$

By substituting the total shear stress and viscous shear stress $\tau_{v12} \equiv \rho\nu\frac{du(y)}{dy}$ in Eq. (8) and rewriting the result in terms of Re_τ and the wall variables $\tilde{y}$ and $\tilde{u}$, we obtain the momentum equation:

$$\kappa^2 I^{3/4}\tilde{y}^2(\frac{d\tilde{u}}{d\tilde{y}})^2 + \frac{d\tilde{u}}{d\tilde{y}} = 1, \tag{10}$$

where $I \equiv I(\eta/y, \tilde{y}/\mathrm{Re}_\tau)$.

Similarly, by taking into account that $\eta = \nu^{3/4}\varepsilon^{-1/4}$ and $\varepsilon = \tau_{t12}\frac{du(y)}{dy}/\rho$ (the energy equation), we obtain a recast form of the energy equation:

$$\eta/y = (\frac{d\tilde{u}}{d\tilde{y}} - (\frac{d\tilde{u}}{d\tilde{y}})^2)^{-1/4}\tilde{y}^{-1}, \tag{11}$$

which is coupled to the momentum equation via the dependence of I on η/y. Eqs. (10) and (11) are the equations of the MVPs for turbulent plane Couette flow.

We proceed following the analysis of Gioia et al. (2010). When the flow is laminar, the turbulent shear stress vanishes ($\tau_{t12} = 0$) and Eq. (10) reduces to $d\tilde{u}/d\tilde{y} = 1$, which is the law of laminar flows (Kundu and Cohen; 2002). When the flow is turbulent, the no-slip boundary condition (Pope; 2000) gives rise to a thin laminar viscous layer next to the wall ($y \ll b$). With the no-slip boundary condition ,that is, $\tilde{u} = 0$ for $\tilde{y} = 0$, the viscous layer solution reads $\tilde{u} = \tilde{y}$. We shall show next that the thickness of the viscous layer can be determined starting with Eqs. (10) and (11).

Consider a point $y \ll b$, $\tau_{t12} > 0$, thus $I = I(\eta/y, 0) > 0$. Then $d\tilde{u}/d\tilde{y}$ can be eliminated from Eqs. (10) and (11) to obtain

$$\tilde{y} = \left(\frac{(\eta/y)^{4/3} + \kappa^{4/3}I^{1/2}(\eta/y, 0)}{\kappa^{2/3}(\eta/y)^{8/3}I^{1/4}(\eta/y, 0)}\right)^{1/2}. \tag{12}$$

Now, for a given value of κ and a given value of β_d, Eq. (12) gives $\tilde{y}$ as a function of η/y. As it turns out, this function has a minimum, denoted $\tilde{y}_v$ (Fig. 5), with the implication that for $\tilde{y} < \tilde{y}_v$ there is no turbulent solution (Gioia et al.; 2010). Thus, for $\tilde{y} < \tilde{y}_v$ the only possible solution is the viscous solution, $\tilde{u} = \tilde{y}$, and $\tilde{y}_v$ represents the thickness of the viscous layer. For $\kappa = 0.81$ and $\beta_d = 7$, we obtain $\tilde{y}_v = 4.2$ (Fig. 5). For $\tilde{y} > \tilde{y}_v$, turbulence prevails and the turbulent MVP can be computed by integrating Eq. (10) with boundary condition $\tilde{u} = \tilde{y}_v$ at $\tilde{y} = \tilde{y}_v$. Note that the MVP is determined by all three parameters (κ, β_d and β_e) whereas the thickness of the viscous layer depends only on κ and β_d.

From the equations above, it is apparent that the standard model of the spectrum should in itself be sufficient to compute, with no additional assumptions, the turbulent MVP corresponding to any given Reynolds number, over the entire domain of flow. Indeed, the model yields complete MVPs with viscous layer, buffer layer, log layer, and

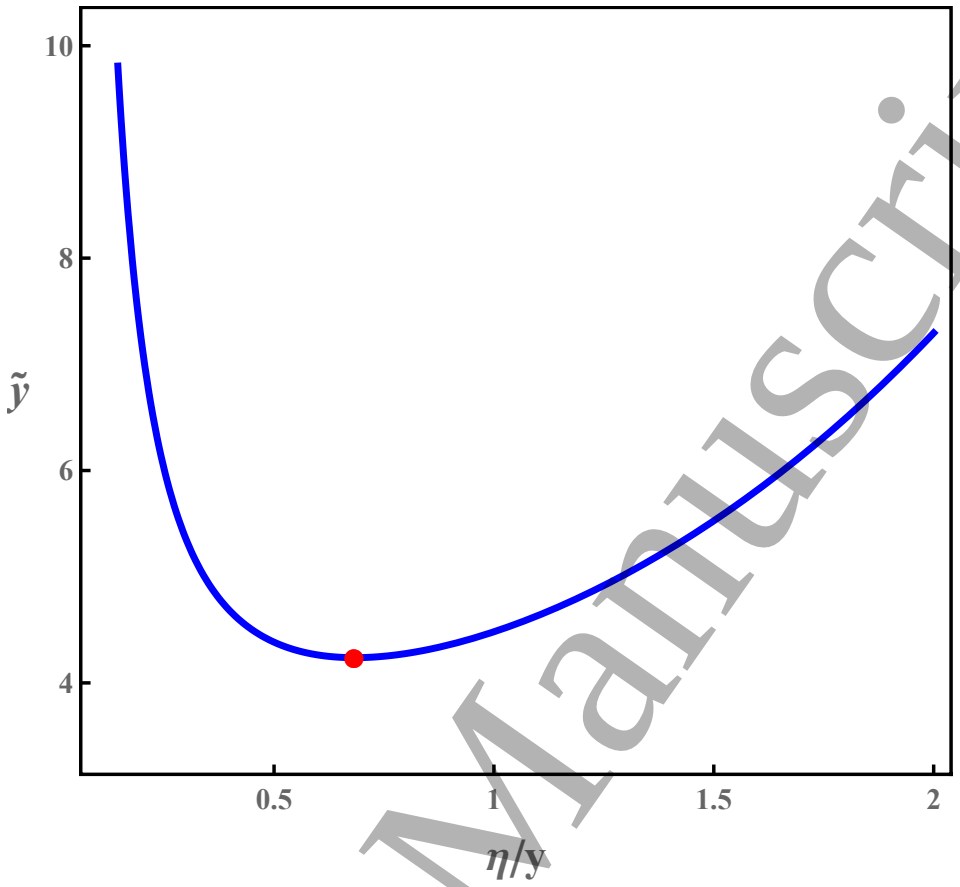

FIG. 5. Plot of $\tilde{y}$ vs. η/y as per Eq. (12), for $\kappa = 0.81$ and $\beta_d = 7$. The thick red dot indicates the point where $\tilde{y}$ is minimized; the minimum is denoted by $\tilde{y}_v$ and represents the thickness of the viscous layer.

wake (Gioia et al.; 2010). Furthermore, *each part of the MVP relates to a specific spectral range*: the viscous layer to the dissipative range, the buffer layer to the dissipative range, the log layer to the inertial range, and the wake to the energetic range (Gioia et al.; 2010).

The one-to-one correspondence between the layers of the MVPs and the ranges of the spectrum plays a crucial role in our analysis of turbulent plane Couette flow. Specifically, in section I we noted that the disparities in the f–Re relation are reflected in only the wakes of the MVPs. In the spectral model the amplitude of the wake is set by only one spectral parameter: the dimensionless parameter β_e of the energetic-range correction. In the next section we turn to how this single parameter can shed light on the disparities.

Before discussing the results, we note that here our emphasis will be on that which the spectrum may tell us about the salient qualitative features of the disparities rather than on how accurately the spectral model can reproduce, on the basis of the standard model of the spectrum, plots of the empirical data on these disparities. In particular, our interest will be on qualitative, or generic, aspects of the energetic-range correction

and their relation to salient characteristics of the wake, notably the relation between the generic fact that the energetic-range correction decays for small k, and the concomitant fact that the MVP overshoots the log law in the wake §. We are not considering the specific form of the energetic-range correction and the exact shape of the overshooting wake. Keeping this outlook in mind, we will not try to fit the f–Re curves and the MVPs from the spectral model (computed using the standard model) to that from empirical data. Instead we will show the computed and the empirical ones in separate yet readily-comparable plots, and focus on the capacity of the spectral model to reproduce all of the salient features of the empirical data, allowing us to trace the cause of each one of those salient features to the corresponding feature of the spectrum.

4. Analysis

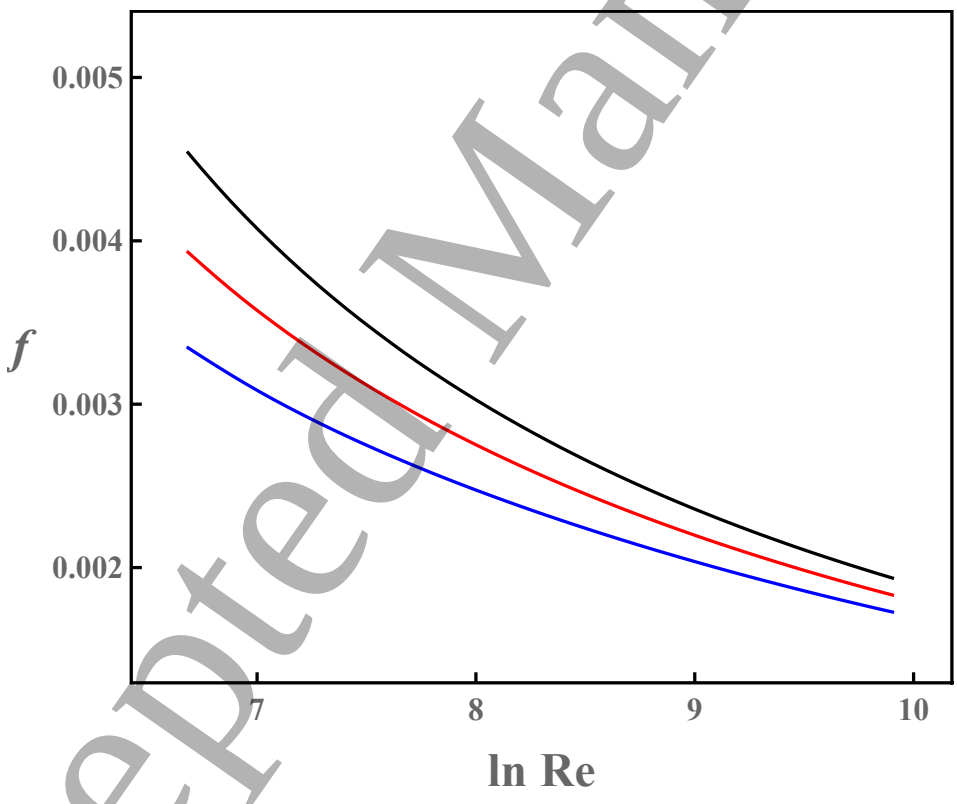

FIG. 6. Log-linear plots of the friction factor of plane Couette flow as a function of Re computed from the spectral model with $\kappa = 0.81, \beta_d = 7$, and three different values of β_e: $\beta_e = 1$ (black line), $\beta_e = 2$ (red line), $\beta_e = 3$ (blue line).

We use the spectral model of the previous section to make the theoretical predictions shown in Figs. 6 and 7. The different curves correspond to different values of the dimensionless parameter β_e. Note that the spectral model can reproduce all of the salient

§ Analysis of such generic aspects of the spectrum can be used to shed light on the scaling relations for the MVPs (Gioia and Chakraborty; 2017).

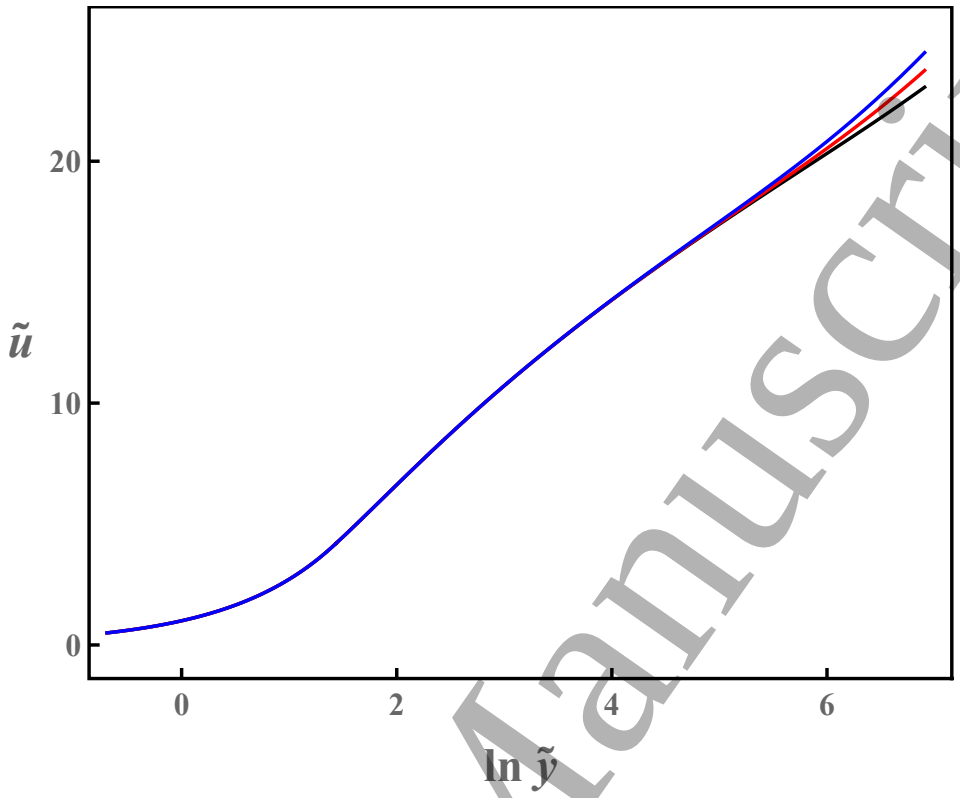

FIG. 7. Log-linear plots of the MVPs of plane Couette flow at the same value of $\mathrm{Re}_\tau = 1000$ computed from the spectral model with $\kappa = 0.81, \beta_d = 7$, and three different values of β_e: $\beta_e = 1$ (black line), $\beta_e = 2$ (red line), $\beta_e = 3$ (blue line).

trends in the experimental and computational data (also shown in Figs. 1 and 2). Since the disparities in friction factor and the attendant disparities in the wakes are accounted for by a single parameter, β_e, of the energetic-range correction, we conclude that the multiple turbulent states we introduced in section I can only differ at the lengthscales of the energetic-range correction, the largest lengthscales of the flow. Experimental and DNS studies of plane Couette flows (Tsukahara et al.; 2006; Avsarkisov et al.; 2014; Lee and Moser; 2018) show that these largest lengthscales appear as counter-rotating, streamwise vortices. While, to our knowledge, there is no systematic study of how these vortices are affected by details of the flow, we posit that the different turbulent states correspond to different configurations of the vortices, which are affected by flow details such as finite-domain effects or the initial conditions. We submit that such a study would shed important insight into plane Couette flows.

From our results we note that, contrary to the view that multiple turbulent states might be somewhat at odds with the phenomenological theory of turbulence, which view was put forward in a discussion of multiple turbulent states in Taylor-Couette flow (Huisman et al.; 2014; van der Veen et al.; 2016), but might be thought applicable to plane Couette flow as well, the difference between any one such state and another is totally circumscribed to the largest lengthscales in the flow. This implies that, at any

given Reynolds number, all turbulent states are indistinguishable at inertial and viscous lengthscales, and that small-scale universality (Kolmogórov; 1941; Liao and Su; 2015; Schumacher et al.; 2014) holds regardless of state, in accord with the phenomenological theory.

4.1. Disparities in macroscopic properties other than the MVPs

As per the spectral model, a higher value of β_e indicates stronger finite-domain effects and results in a lower friction factor and a larger overshooting in the wakes of the MVPs (Figs. 6 and 7). From this conclusion we expect that a change in turbulent state (and the attendant change if the f–Re relation) should have a marked effect on the turbulent velocity fluctuation profile $V(y) \equiv \overline{u_i' u_i'}$; this is because most of the turbulent energy is carried by the largest turbulent eddies in the flow. Indeed, we can predict that a turbulent state with a lower friction factor corresponds to stronger finite-domain effects, which in turn should correspond to higher turbulent velocity fluctuations. This prediction is confirmed in Fig. 9, where we plot the most recent DNS and experimental data, for the highest available values of Re, on the $\tilde{V}(\tilde{y})$ profile, where $\tilde{V} \equiv V/u_\tau^2$.

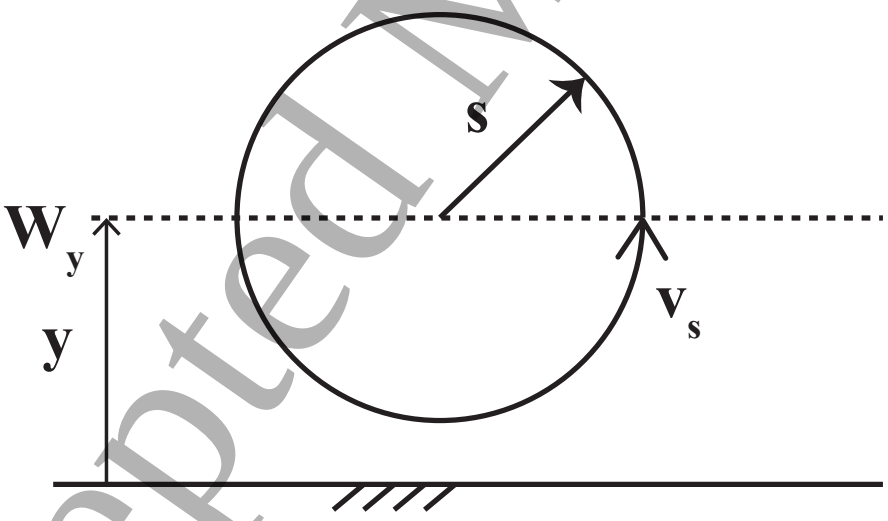

FIG. 8. Schematic used to derive the expression for the turbulent wall-normal velocity fluctuation $v_{rms}(y)$.

The spectral model does not directly give the turbulent velocity fluctuations. However, the turbulent wall-normal velocity fluctuation $v_{rms}(y)$ profile may be identified as v_y (the characteristic velocity of the dominant eddy at a distance y from the wall): in Fig. 8, we consider that at a distance y from the wall, the turbulent wall-normal velocity fluctuation results mostly from the turbulent eddies centering at the wetted surface W_y. Then, the dominant eddies contributing to the turbulent wall-normal velocity fluctuation

$v_{rms}(y)$ must be of size $s = y$ as v_s is a monotonically increasing function of s. Thus, we assume that the $v_{rms}(y) = v_y$. From Eqs. (7) and (8), v_y (or $v_{rms}(y)$) can be directly computed from the spectral model as

$$v_y = v_{rms}(y) = (\kappa^2 \kappa_\varepsilon)^{1/3} I^{3/4} y \frac{du(y)}{dy}. \tag{13}$$

We now are ready to compare our theoretical results of $v_{rms}(y)$ to the corresponding experimental and computational data. Similar to the $V(y)$ profile, the $\tilde{v}_{rms}(\tilde{y})$ profile, where $\tilde{v}_{rms} \equiv v_{rms}/u_\tau$, should also differ depending on the turbulent state. What we expect is that because of weaker finite-domain effects, a higher friction factor should also correspond to a higher turbulent wall-normal velocity fluctuation, which is again confirmed by Fig. 10 and can be reproduced by the spectral model by varying the dimensionless parameter β_e of the energetic-range correction (Fig. 11).

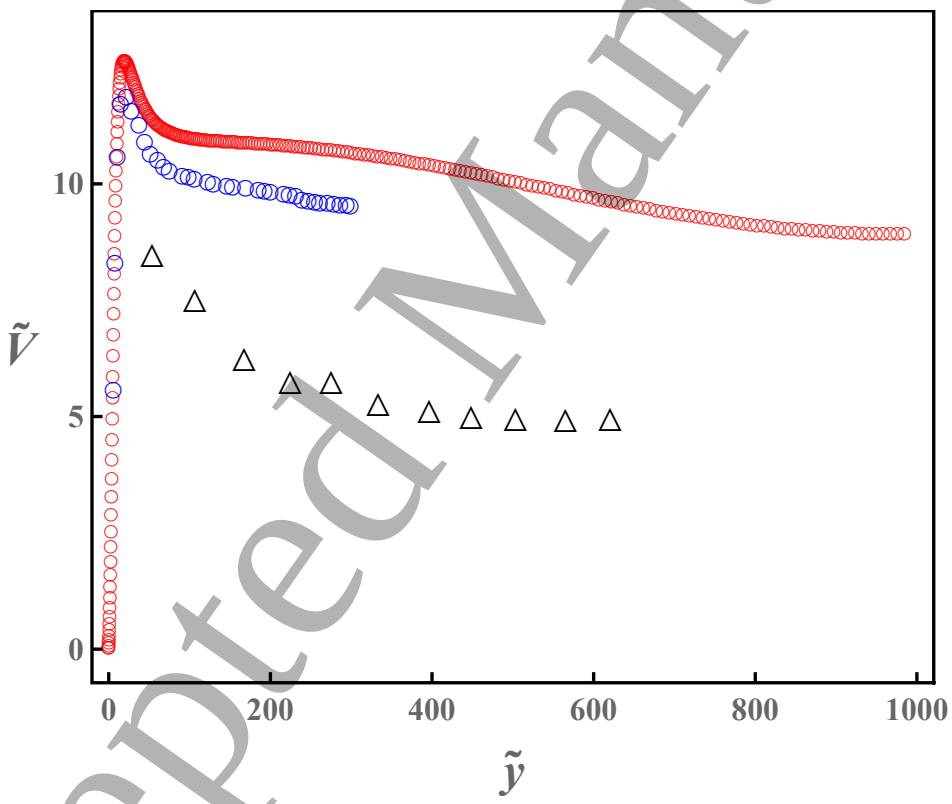

FIG. 9. Plots of experimental and computational data on the turbulent velocity fluctuation profiles of turbulent plane Couette flow. △ $\mathrm{Re}_\tau = 805$ (Telbany and Reynolds; 1982). ◯ DNS from Avsarkisov et al. (2014) (Blue) at $\mathrm{Re}_\tau = 550$, and Pirozzoli et al. (2014) (Red) at $\mathrm{Re}_\tau = 986$, respectively.

5. A note on the asymptotic value of the velocity slope at the flow centerline

In plane Couette flow, the value of the non-dimensional velocity slope at the flow centerline, R_s, has elicited considerable interest since the 1950s when the classical

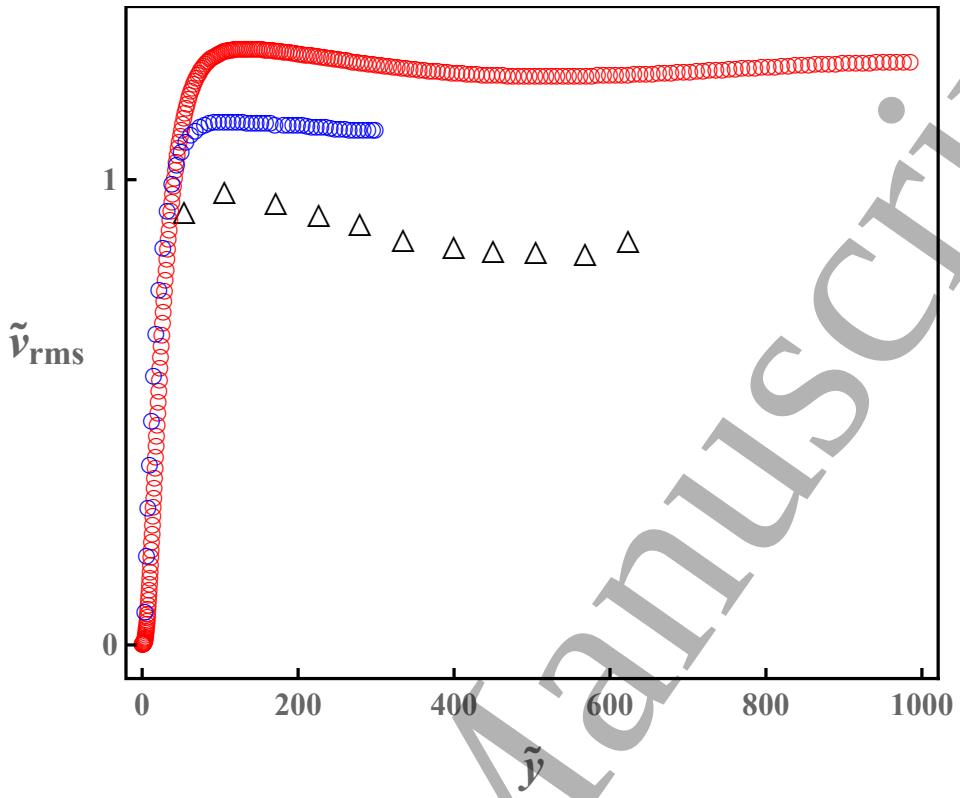

FIG. 10. Plots of experimental and computational data on the turbulent wall-normal velocity fluctuation profiles of turbulent plane Couette flow. △ $\mathrm{Re}_\tau = 805$ citeptelbany. ◯ DNS from Avsarkisov et al. (2014) (Blue) at $\mathrm{Re}_\tau = 550$, and Pirozzoli et al. (2014) (Red) at $\mathrm{Re}_\tau = 986$, respectively.

experiments on turbulent Couette flow were conducted by Reichardt (1956, 1959). Regarding how R_s varies with Re (Fig. 3), while most recent DNS studies report a slow decrease of R_s with increasing Re, different trends have been reported in various experiments. The discrepancies have been attributed to the difficult measurements of small velocity differences in experiments (Pirozzoli et al.; 2014). Regarding whether the value of R_s will approach a constant in the limit of infinite Re, a convincing conclusion has never been reached because of the limitation to achieve very high Reynolds number in both experiments and simulations. Thus, the value of the non-dimensional velocity slope at the flow centerline remains an open question till now. An alternative definition of the non-dimensional velocity slope at the flow centerline is

$$S_0 \equiv \frac{b}{u_c}\frac{du}{dy}|_{y=b} \equiv \frac{d\tilde{u}}{d\ln\tilde{y}}|_{\tilde{y}=\mathrm{Re}_\tau}\sqrt{f} = R_s\sqrt{f}. \tag{14}$$

Here, the spectral model will be employed to address the open question on the value of the non-dimensional velocity slope at the flow centerline of plane Couette flow. R_s and S_0 are readily to be calculated from the theoretically computed MVP and friction factor. At the flow centerline where the viscous shear stress is negligible, Eq. (10) gives that $R_s = I_0^{-3/8}/\kappa$, where $I_0 \equiv I(\eta/b, 1)$, which depends on Re via η/b. For a high enough Reynolds number, η/b reduces to zero. Thus $I_0 = I(0, 1)$ is not dependent on

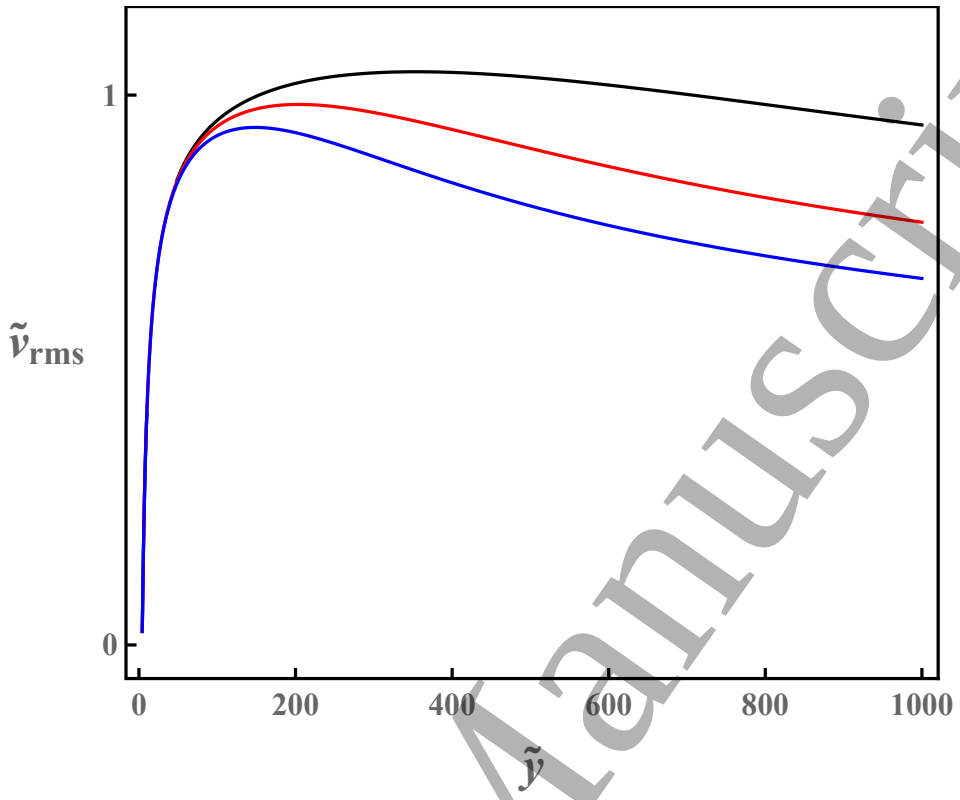

FIG. 11. Plots of the turbulent wall-normal velocity fluctuation profiles of plane Couette flow at the same value of $\mathrm{Re}_\tau = 1000$ computed from present spectral model with $\kappa = 0.81, \beta_d = 7$, and three different values of β_e: $\beta_e = 1$ (black line), $\beta_e = 2$ (red line), $\beta_e = 3$ (blue line).

Re any more and R_s becomes a constant value, which is determined by the energetic-range correction to the spectrum via $I(0,1)$. Note that the conclusion that R_s becomes a constant value at high Reynolds numbers is valid regardless of the form of the function $I(\eta/s, s/b)$, thus regardless of the form of the energetic-range correction to the spectrum, as long as the energetic-range correction to the spectrum is a function of s/b. In the standard model of the spectrum we are using here, the dimensionless parameter β_e of the energetic-range correction sets the constant value of R_s at high Reynolds numbers (Fig. 12) as I_0 becomes

$$I(0,1) \equiv \frac{2}{3}\int_1^\infty \xi^{-5/3}(1+\beta_e^2/\xi^2)^{-17/6}d\xi, \tag{15}$$

which is a constant value only depending on β_e. We have argued that a certain β_e signifies a specific turbulent state of plane Couette flow. That is to say, for each turbulent state, there is an asymptotic constant value of R_s in the limit of high Re as shown in Fig. 12.

In Fig. 13, we also plot $S_0 \equiv R_s\sqrt{f}$ as a function Re. The decreasing rate of S_0 is getting slow in high Reynolds number region as the friction factor f is decreasing slowly. At infinite Reynolds number, if the friction factor becomes zero, then S_0 will be zero.

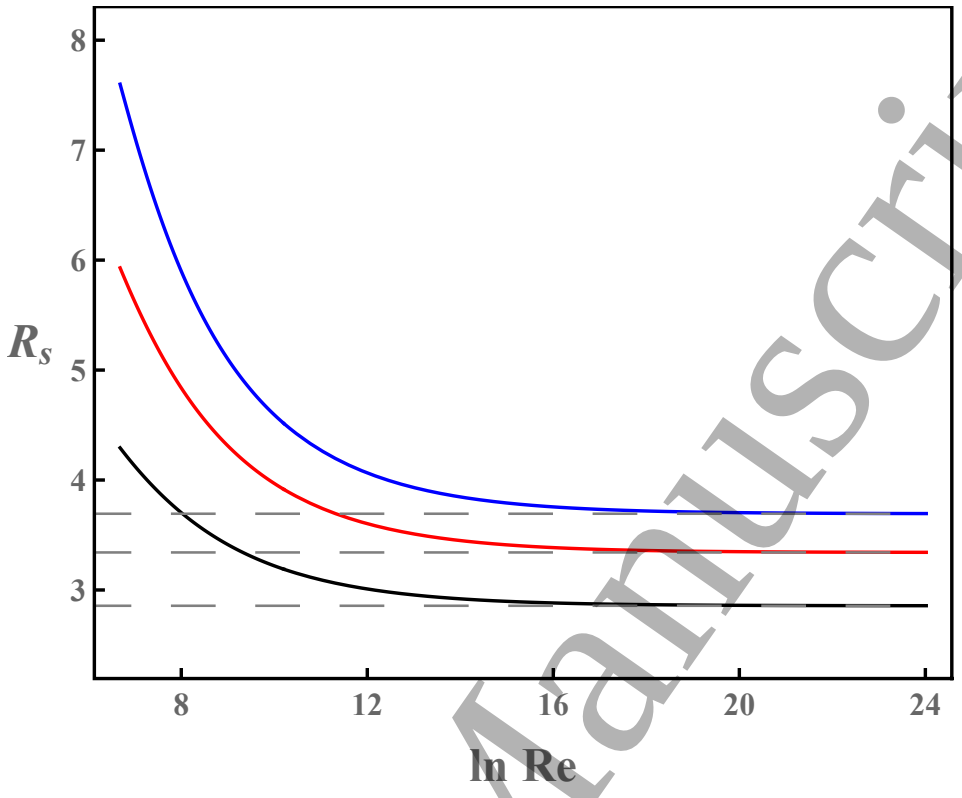

FIG. 12. Log-linear plots of the non-dimensional velocity slope at the flow centerline R_s of plane Couette flow as a function of Re computed from present spectral model with $\kappa = 0.81, \beta_d = 7$, and three different values of β_e: $\beta_e = 1$ (black line), $\beta_e = 2$ (red line), $\beta_e = 3$ (blue line). The dashed grey lines denote that at high Reynolds numbers, the constant values of $R_s = 2.86, 3.34$, and 3.69 for $\beta_e = 1$, $\beta_e = 2$, and $\beta_e = 3$, respectively.

6. Discussion and summary

We have used the spectral model of the MVPs of turbulent plane Couette flow to revisit the Reichardt–Robertson disparity, with the following conclusions.

(i) The Reichardt–Robertson disparity is a manifestation of the existence of multiple turbulent states in turbulent plane Couette flow.

(ii) By invoking the one-to-one, or *bijective* property of the spectral link, whereby each successive range of the spectrum of turbulent kinetic energy relates to one, and only one, of the successive layers of the attendant MVP (the dissipative range to the buffer layer, the inertial range to the log layer, and the energetic range to the wake), we have been able to ascertain the ways in which these multiple turbulent states differ from one another, namely only at the largest lengthscales in the flow, corresponding to the energetic range of the eddy velocity distribution.

(iii) Corollary: a change in turbulent state can only alter the wake of the attendant MVP (which is the part of the MVP dominated by the eddies of the energetic range).

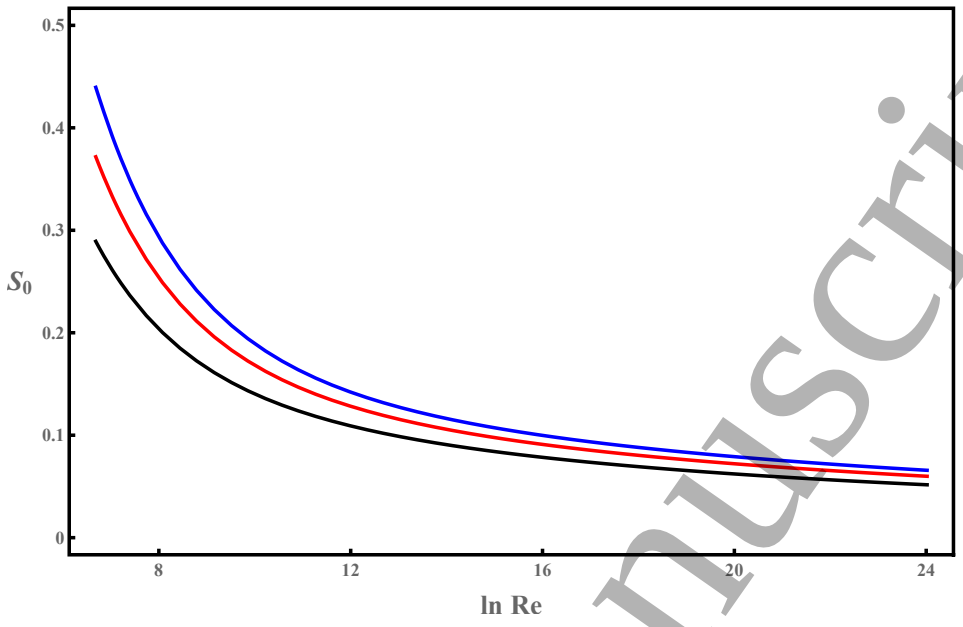

FIG. 13. Log-linear plots of the non-dimensional velocity slope at the flow centerline S_0 of plane Couette flow as a function of Re computed from present spectral model with $\kappa = 0.81, \beta_d = 7$, and three different values of β_e: $\beta_e = 1$ (black line), $\beta_e = 2$ (red line), $\beta_e = 3$ (blue line).

(iv) At smaller lengthscales, comprising the inertial and viscous portions of the spectrum of turbulent kinetic energy, the spectrum is one and the same regardless of the turbulent state, consistent with the phenomenological theory of turbulence.

(v) Thus, the existence of multiple turbulent states does not contradict the universality of the spectrum of turbulent kinetic energy (such as this universality is understood in the phenomenological theory).

(vi) Conversely, spectral universality does not rule out the existence of multiple turbulent states.

These conclusions might apply beyond plane Couette flow to a general class of flows engendered by moving boundaries. Consider, for instance, the recent papers on multiple states in highly turbulent Taylor-Couette flows (Huisman et al.; 2014; van der Veen et al.; 2016). These studies report two branches of global torque, which is analogous to the friction factor f. These branches correspond to differences in the wake of the MVPs of azimuthal velocity and differences in the size of large-scale Taylor vortices, which correspond to differences in the energetic-range corrections to the spectrum. Our analysis might provide a unified explanation for these features.

This work was supported financially by the University of South China and Okinawa Institute of Science and Technology Graduate University. The author is greatly thankful fo Professor Gustavo Gioia and Professor Pinaki Chakraborty for a number of illuminating suggestions.

References

Avsarkisov, V., Hoyas, S., Oberlack, M. and Garcia-Galache, J. P. (2014). Turbulent plane Couette flow at moderately high Reynolds number, *J. Fluid Mech.* **751**: R1–10.

Bech, K. H., Tillmark, N., Alfredsson, P. and Anderson, H. I. (1995). An investigation of turbulent plane Couette flow at low Reynolds numbers, *J. Fluid Mech.* **286**: 291–325.

Furuichi, N., Terao, Y., Wada, Y. and Tsuji, Y. (2015). Friction factor and mean velocity profile for pipe flow at high Reynolds numbers, *Phys. Fluids* **27**(9): 095108.

Gioia, G. and Chakraborty, P. (2006). Turbulent friction in rough pipes and the energy spectrum of the phenomenological theory, *Phys. Rev. Lett.* **96**: 044502.

Gioia, G. and Chakraborty, P. (2017). Spectral derivation of the classic laws of wall-bounded turbulent flows, *P. Roy. Soc A-Math. Phy.* **473**(2204): 20170354.

Gioia, G., Guttenberg, N., Goldenfeld, N. and Chakraborty, P. (2010). Spectral theory of the turbulent mean-velocity profile, *Phys. Rev. Lett.* **105**: 184501.

Huisman, S. G., Veen, R. C., Sun, C. and Lohse, D. (2014). Multiple states in highly turbulent Taylor-Couette flow, *Nat. Commun.* **5**(3820).

Kitoh, O., Nakabyashi, K. and Nishimura, F. (2005). Experimental study on mean velocity and turbulence characteristics of plane Couette flow: low-Reynolds-number effects and large longitudinal vortical structure, *J. Fluid Mech.* **539**: 199–227.

Kolmogórov, A. N. (1941). The local structure of turbulence in incompressible viscous fluid for very large Reynolds numbers, *Dokl. Akad. Nauk SSSR* **30**: 301–305.

Kundu, P. K. and Cohen, I. M. (2002). *Fluid Mechanics*, second edn, Academic Press, San Diego, CA.

Lee, M. J. and Kim, J. (1991). The structure of turbulence in a simulated plane Couette flow, *8th Symposium on Turbulent Shear Flows, Munich, Federal Republic of Germany, Sept. 9-11, 1991, Proceedings. Vol. 1*, University Park, PA, pp. 531–536.

Lee, M. and Moser, R. D. (2018). Extreme-scale motions in turbulent plane couette flows, *J. Fluid Mech.* **842**: 128–145.

Liao, Z.-J. and Su, W.-D. (2015). Kolmogórov's hypotheses and global energy spectrum of turbulence, *Phys. Fluids* **27**(4): 041701.

Pirozzoli, S., Bernardini, M. and Orlandi, P. (2014). Turbulence statistics in Couette flow at high Reynolds number, *J. Fluid Mech.* **758**: 327–343.

Pope, S. B. (2000). *Turbulent Flows*, Cambridge University Press, Cambridge, England.

Prandtl, L. (1953). *Essentials of Fluid Dynamics*, 3rd edn, Blackie & Son, London.

Reichardt, H. (1956). Über die geschwindigkeitsverteilung in einer geradlinigen turbulenten Couetteströmung, *Z. Angew. Math. Mech. Sonderheft* **36**: S26–29.

Reichardt, H. (1959). Gesetzmässigkeiten der geradlinigen turbulenten Couetteströmung, Mitt. Max-Planck-Inst. für Strömungsforschung, No. 22, Göttingen.

Robertson, J. M. (1959). On turbulent plane-Couette flow, *Proceedings of the Sixth Midwest Conference on Fluid Mechanics*, University of Texas, Austin, pp. 169–182.

Robertson, J. M. and Johnson, H. F. (1970). Turbulence structure in plane Couette flow, *Proc. A.S.C.E., J. Eng. Mech.* **96**: 1171–1182.

Schumacher, J., Scheel, J. D., Krasnov, D., Donzis, D. A., Yakhot, V. and Sreenivasan, K. R. (2014). Small-scale universality in fluid turbulence, *Proc. Natl. Acad. Sci. USA* **111**(30): 10961–10965.

Telbany, M. M. M. E. and Reynolds, A. J. (1982). The structure of turbulent plane Couette flow, *Trans. A.S.M.E., J. Fluids Eng.* **104**: 367–372.

Tennekes, H. and Lumley, J. L. (1972). *A First Course in Turbulence*, MIT Press, Cambridge, MA and London.

Tsukahara, T., Kawamura, H. and Shigai, K. (2006). DNS of turbulent Couette flow with emphasis on the large-scale structure in the core region, *J. Turbul.* **7**(19).

van der Veen, R. C., Huisman, S. G., Dung, O.-Y., Tang, H. L., Sun, C. and Lohse, D. (2016). Exploring the phase space of multiple states in highly turbulent Taylor-Couette flow, *Phys. Rev. Fluids* **1**(2): 024401.

Vincenti, W. G. (1982). Control-volume analysis: A difference in thinking between engineering and physics, *Technol. Cult.* **23**(2): 145–174.